A&A 469, 1211–1219 (2007)
DOI: 10.1051/0004-6361:20077359

Astronomy & Astrophysics

An X-ray survey in SA 57 with XMM-Newton⋆,⋆⋆

D. Trevese[1], F. Vagnetti[2], S. Puccetti[3,4], F. Fiore[4], M. Tomei[1], and M. A. Bershady[5]

[1] Dipartimento di Fisica, Universitá di Roma "La Sapienza", P.le A. Moro 2, 00185 Roma, Italy
e-mail: dario.trevese@roma1.infn.it
[2] Dipartimento di Fisica, Universitá di Roma "Tor Vergata", via delle Ricerca Scientifica 1, 00133 Roma, Italy
[3] ASI Science Data Centre, c/o ESRIN, via G. Galilei, 00044 Frascati, Italy
[4] INAF – Osservatorio Astronomico di Roma, via di Frascati 33, 00040 Monte Porzio Catone, Italy
[5] Department of Astronomy, University of Wisconsin, 475 North Charter Street, Madison, WI 53706, USA

Received 26 February 2007 / Accepted 17 April 2007

ABSTRACT

Context. The maximum number density of Active Galactic Nuclei (AGNs), as deduced from X-ray studies, occurs at $z \lesssim 1$, with lower luminosity objects peaking at smaller redshifts. Optical studies lead to a different evolutionary behaviour, with a number density peaking at $z \approx 2$ independently of the intrinsic luminosity, but this result is limited to active nuclei brighter than the host galaxy. A selection based on optical variability can detect low luminosity AGNs (LLAGNs), where the host galaxy light prevents the identification by non-stellar colours.
Aims. We want to collect X-ray data in a field where it exists an optically-selected sample of "variable galaxies", i.e. variable objects with diffuse appearance, to investigate the X-ray and optical properties of the population of AGNs, particularly of low luminosity ones, where the host galaxy is visible.
Methods. We observed a field of 0.2 deg^2 in the Selected Area 57, for 67 ks with XMM-Newton. We detected X-ray sources, and we correlated the list with a photographic survey of SA 57, complete to $B_J \sim 23$ and with available spectroscopic data.
Results. We obtained a catalogue of 140 X-ray sources to limiting fluxes 5×10^{-16}, 2×10^{-15} erg cm^{-2} s^{-1} in the 0.5–2 keV and 2–10 keV respectively, 98 of which are identified in the optical bands. The X-ray detection of part of the variability-selected candidates confirms their AGN nature. Diffuse variable objects populate the low luminosity side of the sample. Only 25/44 optically-selected QSOs are detected in X-rays. 15% of all QSOs in the field have X/O < 0.1.

Key words. surveys – galaxies: active – galaxies: quasars: general – X-rays: galaxies

1. Introduction

Supermassive black holes (SMBHs) are believed to inhabit most, if not all, bulges of present-epoch galaxies (Kormendy & Richstone 1995), and strong evidences exist of a correlation between the black hole mass and either the mass and luminosity (Marconi & Hunt 2003, and refs. therein) or the velocity dispersion of the host bulge (Ferrarese & Merrit 2000; Tremaine et al. 2002). This strongly suggests that the formation and growth of SMBHs and galaxies are physically related processes. A theory of cosmic structure formation and the nature of the Active Galactic Nuclei (AGN) feedback (Silk & Rees 1998; Cavaliere & Vittorini 2002; Vittorini et al. 2005) requires the knowledge of the evolution in cosmic time of the AGN population.

In recent years consensus has grown on a fast increase of the number density of QSOs moving forward in cosmic time, until $z \sim 3$, followed by a slower decline of the luminosity function (LF), which can be described by a QSO luminosity evolution. The quantification of this behaviour is currently based on the 2QZ survey (Croom et al. 2001) for $z < 2.5$, on Warren et al. (1994) and Schmidt et al. (1995) surveys for $z \geq 3$ and on the Sloan Digital Sky Survey (SDSS) data for $z > 4.5$ (Fan et al. 2001; Anderson et al. 2001). None of the above surveys covers the redshift region where the maximum of QSOs density is located. Moreover, higher redshift data are restricted to the bright end of QSO LF and even low redshift data do not sample the evolution of objects fainter than $M_B < -23$.

Wolf et al. (2003) analyse the intermediate redshift region, where the maximum in cosmic time of the number-density of AGNs is located ($z \sim 2$). They use a sample selected by a multiband technique, and extend the study down to $M_B \simeq -21.5$. They provide the most accurate measurement available to date of the maximum in cosmic time of the AGN comoving space density. However their method cannot select fainter AGNs due to the contribution of the host galaxy light to the observed spectral energy distribution. Variability was adopted as a tool to select a sample of QSOs with point-like images in SA 57, on the basis of a collection of photographic plates taken at the Mayall 4 m KPNO telescope about once per year for 15 consecutive years (Trevese et al. 1989). This technique is well suited for selection of intrinsically low luminosity AGNs (LLAGNs), since variability is higher in AGNs of lower luminosity (Trevese et al. 1994; Hook et al. 1994; Cristiani et al. 1996; Vanden Berk et al. 2004). For these reasons a sample of "variable galaxies", i.e. variable objects with extended images, was created from the same plates of SA 57 (Bershady et al. 1998, (BTK)). Spectroscopic observations have already confirmed the AGN nature of 5 relatively bright ($B_J < 22.5$) objects, and provided redshifts in the range

⋆ Based on observations obtained with XMM-Newton, an ESA science mission with instruments and contributions directly funded by ESA Member States and NASA.

⋆⋆ Table 2 is only available in electronic form at CDS via anonymous ftp to cdsarc.u-strasbg.fr (130.79.128.5) or via http://cdsweb.u-strasbg.fr/cgi-bin/qcat?J/A+A/469/1211

$0.2 < z < 0.4$ and absolute B magnitudes $-22.5 < M_B < -19.0$. Subsequently, Sarajedini et al. (2003) selected galaxies with variable nuclei in the Hubble Deep Field, showing that a sizable fraction of them is undetected in the X-rays even at the flux limits of the 2Ms Chandra Deep Field North Survey (Alexander et al. 2003). Thus, optical variability is a good complementary AGN selection criterion, which is also competitive, with respect to X-ray surveys, to efficiently find high sky densities of AGNs (Brandt & Hasinger 2005).

Hard X-ray observations are the most efficient way to discriminate between accretion-powered sources, such as AGN, from starlight and optically thin, hot-plasma emission. Deep surveys have resolved 80–90% of the 2–10 keV Cosmic X-ray Background (CXB) into sources (Moretti et al. 2003; Brandt & Hasinger 2005; Hickox & Markevitch 2006). While these studies are, at least qualitatively, confirming the predictions of standard AGN synthesis models for the CXB (e.g. Comastri et al. 2001), somewhat surprising results are also emerging: i) the sources making the CXB have a maximum number density at a redshift ($z \sim 1$), lower than predicted by synthesis models (e.g. Hasinger 2003); ii) there is evidence of a strong luminosity dependence to the evolution, with low luminosity sources (i.e. Seyfert galaxies) peaking at a significantly later cosmic time than high luminosity ones (Hasinger 2003; Cowie et al. 2003; Fiore et al. 2003; La Franca et al. 2005). However, a direct comparison with the optical LF evolution requires to extend the latter down to $M_B \sim -19$, i.e. in the range of the BTK sample.

For this reason we have performed a medium-deep observation of the same field in the SA 57 which is one of the best studied fields of the sky at all wavelengths: radio FIRST Survey (Becker et al. 1995), IR deep ISOPHOT Survey (Linden-Vornle et al. 2000), soft X-ray ROSAT HRI (Miyaji et al. 1997). A field of ∼35 arcmin in diameter has been repeatedly observed since 1975 in the U, B_J, F, N bands. A number of search techniques, including non-stellar colour, absence of proper motion and variability have been applied in this field for the detection of QSOs/AGNs to faint limits (Koo et al. 1986; Koo & Kron 1988; Trevese et al. 1989, 1994; Bershady et al. 1998).

We observed the central area of SA 57 with XMM-Newton with the aim of performing a combined X-ray and optical analysis of the sources detected in the field. As a result we produced a catalogue of 140 X-ray sources. In the present paper we report on the results of these observations and the optical identification made possible by the already existing photometric and spectroscopic data. This allows a break down of a substantial fraction of the X-ray sample into normal galaxies, different types of Seyfert galaxies, QSOs and possibly obscured *quasar-2* type objects.

The paper is organised as follows. Section 2 describes the X-ray sample, Sect. 3 discusses the known optical sources, both detected and undetected in X-rays, Sect. 4 discusses the results, Sect. 5 contains a summary.

Consensus cosmology, $H_0 = 75\ \mathrm{km\,s^{-1}\ Mpc^{-1}}$, $\Omega_\mathrm{m} = 0.3$, $\Omega_\Lambda = 0.7$ is adopted throughout the paper.

2. X-ray sources

A deep XMM-Newton pointing covers the SA57 region. The pointing was centred at $\alpha = 13^\mathrm{h}08^\mathrm{m}28^\mathrm{s}$ and $\delta = 29°23'07''$ (J2000). The X-ray observations were performed on January 2005 with the European Photon Imaging Camera (EPIC: one PN-CCD camera (0.5–10 keV, Struder et al. 2001) and two MOS-CCD cameras (MOS1, MOS2, 0.3–10 keV, Turner et al. 2001). Table 1 gives a log of the XMM-Newton observations.

Table 1. Observation log.

Instrument	Exposure [ks]	Net exposure [ks][a]
PN	62	45
MOS1	67	49
MOS2	67	51

[a] Net on-axis exposure time after rejection of high background periods (see Sect. 2).

The data have been processed using the XMM-Newton Science Analysis Survey (SAS) v.6.0. We used the event files linearised with a standard reduction pipeline (Pipeline Processing System, PPS) at the Survey Science Centre (SSC, University of Leicester, UK). Events spread at most in two contiguous pixels for PN (i.e. pattern = 0–4) and in four contiguous pixels for MOS (i.e., pattern = 0–12) have been selected. Event files were cleaned from bad pixels (hot pixels, events out of the field of view, etc.) and the soft proton flares following Puccetti et al. (2006).

Source detection was performed on co-added (in sky coordinates) PN+MOS1+MOS2 images accumulated in four energy bands: 0.5–10 keV (total band, T), 0.5–2 keV (soft band, S), 2–10 keV (hard band, H), 5–10 keV (ultra hard band, HH).

The source detections and the X-ray photometry were performed by using the PWXDetect code, developed at INAF – Osservatorio Astronomico di Palermo, following Pillitteri et al. (2006). The code is derived from the original ROSAT code for source detection by (Damiani et al. 1997) and allows one to combine data from different EPIC cameras and data taken in different observations, in order to achieve the deepest sensitivity. The code is based on the analysis of the wavelet transform (WT) of the count rate image. A WT of a two-dimensional image is a convolution of the image with a "generating wavelet" kernel, which depends on position and length scale. In the algorithm developed by Damiani et al. (1997), the generating wavelet is a "Mexican hat". The length scale is a free parameter; therefore this method is particularly suited for cases where the point spread function (PSF) is strongly varying across the image, and moreover includes the exposure maps to handle sharp background gradients. It also provides robust detections of extended sources.

To evaluate count rates, we have chosen PN as the reference detector. The scaling factor between PN, MOS1 and MOS2 depends on the relative instrument efficiency and source spectral shape. We used the scaling factors evaluated by Puccetti et al. (2006) for a power law model with an energy index $\alpha_\mathrm{E} = 0.8$.

We adopted a threshold on the significance level corresponding to a probability of 2×10^{-5} that a local maximum is generated by a Poisson fluctuation of the background counts. The limiting fluxes on axis, in the T, S, H and HH bands, are approximately 10^{-15}, 5×10^{-16}, 2×10^{-15}, 10^{-14} erg cm^{-2} s^{-1} respectively. The result of this selection is a sample of 140 sources, detected in at least one band.

For each source, count rates were converted to fluxes adopting constant conversion factors for the S and H bands $f_\mathrm{S} = a_\mathrm{S} c_\mathrm{S}$, $f_\mathrm{H} = a_\mathrm{H} c_\mathrm{H}$, with $a_\mathrm{S} = 1.61 \times 10^{-12}$ erg cm^{-2}, $a_\mathrm{H} = 8.26 \times 10^{-12}$ erg cm^{-2}, corresponding to an "average source spectrum" f_λ^A represented by a power law of energy index $\alpha_\mathrm{E} = 0.8$. Fluxes f_T in the T band are computed as follows: a) if the object is detected in both the S and H bands, $f_\mathrm{T} = f_\mathrm{S} + f_\mathrm{H}$; b) if the object is detected in the T band and in one of the S or H bands, the missing count rate is evaluated as $c_\mathrm{H} = c_\mathrm{T} - c_\mathrm{S}$ or $c_\mathrm{S} = c_\mathrm{T} - c_\mathrm{H}$ respectively, and the flux is computed as above and reported in Table 1 if greater than zero; c) if the object is detected only in

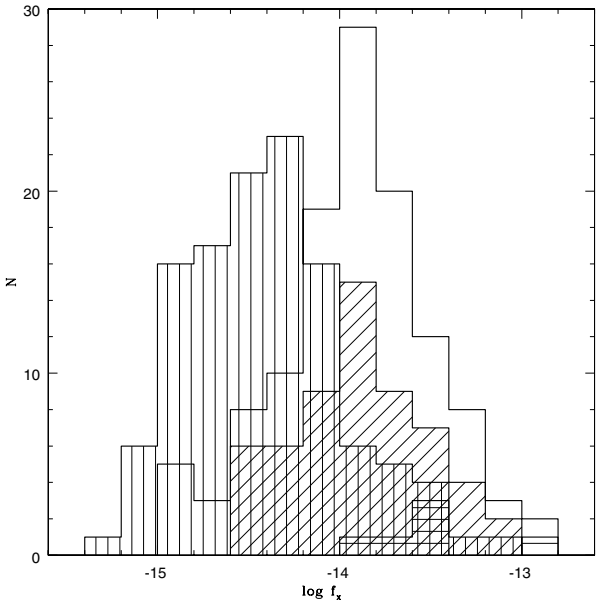

Fig. 1. The flux distribution for the sources detected in the different bands: T band (no shading), S band (vertical shading), H band (diagonal shading), HH band (horizontal shading).

S or H band $f_T = f_S$ or $f_T = f_H$ respectively; d) if the object is detected in the T band only, the flux f_T reported in the table is computed adopting an average conversion factor, $f_T = a_T c_T$ with $a_T = 3.75 \times 10^{-12}$ erg cm^{-2} determined by the linear regression of f_T vs. c_T for all the objects of cases a), b), c). In any of the bands, when the source is not detected and the flux cannot be evaluated from the other bands, a 3-σ upper limit is computed adopting the relevant average conversion factor.

The results are reported in Table 2, where *Col. 1*: catalogue serial number; *Cols. 2, 3*: right ascension and declination (J2000); *Cols. 4–6*: fluxes in the T, S, H bands respectively; *Col. 7*: the identification rank, as defined in the note. 3-σ upper limits are preceded by a "<" character.

Of the 140 sources, the numbers of sources detected in the T, S, H an HH bands are 119, 117, 58, 6 respectively and the relevant histograms are shown in Fig. 1.

On the basis of the optical coordinates of the most secure quasar identifications in the field, a small shift in α and δ has been computed, respect to the (X-ray) detection coordinates, to obtain a more accurate correspondence with our optical coordinate system, based on USNO-A2.0 (see next section).

3. Optical sources

A photographic survey of SA57 was conducted with the prime focus camera at Mayall 4 m telescope at Kitt Peak National Observatory (KPNO) from 1974 to 1989. A photometric catalogue of 8146 objects in U, B_J, F and N bands in a field of ~0.3 deg^2, complete to $B_J \sim 23$ was used for optical identifications of the X-ray detected sources (Kron 1980; Koo 1986). The optical coordinates were recomputed by cross-correlating the SA57 catalogue with USNO-A2.0 catalogue. After a 2-σ rejection, the IRAF *ccmap* utility provides a 4th order coordinate transformation based on 446 objects spread over the field, with <0.2 arcsec rms deviation in both α and δ, respect to USNO-A2.0.

The above multi-epoch observations have been used to select AGN candidates on the basis of variability. In the case of point-like sources, the variability criterion has proven to be 74% complete (variable AGNs/total AGNs), while its reliability (variable AGNs/total variables) is between 80% and 95%, depending on the variability threshold adopted, which in turn is chosen taking into account the photometric accuracy (Trevese et al. 1989). For the extended objects, variability can select AGNs even in cases where color selection is not effective due to dominance of the host galaxy light. A sample of 51 variable extended objects was created by Bershady et al. (1998) (BTK), 16 of which have $B_J < 22.5$. A fraction of them was observed spectroscopically, and 5 objects confirmed their AGN character. A new spectroscopic campaign of SA57 is in progress (Trevese et al. 2007). In the meantime X-ray emission from some of these candidates strongly suggests their AGN nature (see below).

3.1. Optical identification of X-ray sources

The optical identifications are reported in Table 3, where the columns have the following meaning: *Col. 1*: source serial number; *Col. 2*: identification rank (same as Table 2); *Col. 3*: serial number NSER in the optical catalogue of KPNO survey of SA57 (Kron 1980; Koo 1986), or, preceded by a "G", in the NGPFG catalogue (Infante et al. 1995). *Cols. 4, 5*: right ascension and declination (J2000); *Cols. 6, 7*: B_J and F magnitudes respectively; *Col. 8*: redshift; *Col. 9*: source class (as specified in the note).

Identifications indicated with "I" are the most secure and correspond to optical positions within 5 arcsec from the X-ray position, and no other optical objects inside this area. Other marginal or less secure identification, more distant than 5 arcsec, are indicated with "M". When more than one object falls within 5 arcsec from the X-ray position sources are indicated with "A", meaning ambiguous identification. A total of 98 objects has been identified with optical sources. Of these, 72 are most secure identifications (I), 15 are classified as marginal (M), 11 are ambiguous (A). 42 sources are unidentified (U).

Of the 72 most secure identifications 33 are either confirmed or candidate AGNs: 24 confirmed and 3 candidate QSOs, 5 BTK objects (two of which are spectroscopically confirmed), and 1 radio galaxy. Another 7 optically identified X-ray sources correspond to galaxies with spectroscopic redshifts in the catalogue of Munn et al. (1997) of SA 57. One of these corresponds to the cD galaxy in the centre of the galaxy cluster II Zw 1305.4+2941 at $z = 0.241$. Among the AGN candidates selected through variability alone (i.e., not previously selected by other methods), 9 are detected securely in X-rays (4 point-like and 5 extended, see note "e" in Table 3). Of these, 3 are already confirmed by optical spectroscopy. For the remaining 6 objects we can provisionally assume the X-ray detection as a confirmation of their AGN nature, though optical spectroscopy will be eventually necessary to measure their absolute luminosity and assign them to a specific class.

3.2. X-ray undetected optical sources

We have searched the NASA Extragalactic Database (NED) for objects with known redshift and classified as "QSO", in the area covered by our X-ray survey. The resulting list contains 44 objects, 25 of which already appear in Tables 2 and 3 since they are detected in X-rays. The remaining 19 QSOs not detected in X-rays are reported in Table 4. Most of them belong to the

Table 3. Optical identifications.

SA57X	IdRank[a]	NSER[b]	RA(2000)	Dec(2000)	B_J	F	z	Class[c]
4	A	3049	13 08 56.66	29 11 58.9	23.14	21.70		
		3017	13 08 56.68	29 11 57.3	23.03	21.49		
8	I	3544	13 08 49.65	29 12 44.8	20.17	19.91	1.808	Q
9	I	3535	13 07 54.64	29 12 46.3	20.41	19.16	0.403	G
11	I	3927	13 08 52.56	29 13 26.6	22.82	22.14		
12	I	3993	13 08 35.39	29 13 34.6	22.95	22.14		
13	I	4274	13 08 58.44	29 14 02.6	23.82	22.26		
14	M	4290	13 08 29.43	29 14 04.0	24.68			
15	I	4437	13 07 48.90	29 14 17.8	22.13	21.35	0.706	G
17	I	4455	13 07 41.86	29 14 19.2	23.41	23.12		
19	I	4793	13 07 37.48	29 14 52.4	23.91	23.58		
20	I	4811	13 09 00.38	29 14 53.8	22.80	21.32	3.543	Q
21	I	4882	13 08 12.20	29 14 59.1	21.89	21.30	1.468	Q
22	I	4855	13 09 20.52	29 14 58.6	22.35	21.70	1.305	Q
23	I	5141	13 08 27.22	29 15 25.2	20.60	20.16	1.094	Q
25	I	5185	13 08 18.43	29 15 30.0	21.66	21.04		[Q][e]
27	I	5422	13 09 11.88	29 15 52.7	20.62	19.98	1.083	Q
29	I	5643	13 08 15.75	29 16 12.3	21.17	20.74	0.983	Q
30	M	5711	13 08 28.37	29 16 19.0	23.78	22.45		
31	I	5767	13 07 38.11	29 16 26.5	20.60	19.71	0.708	Q
33	I	6442	13 09 04.77	29 17 29.6	22.28	22.62	2.124	Q
34	A	6579	13 08 47.67	29 17 44.6	23.35	23.01		
		6593	13 08 47.27	29 17 46.2	24.51	22.40		
35	I	6669	13 07 49.58	29 17 54.4	22.96	22.31		BTK[e]
37	I	6825	13 08 22.19	29 18 07.8	22.92	21.26		
38	I	6884	13 08 13.52	29 18 12.5	20.83	19.01		
40	I	7251	13 07 58.01	29 18 42.8	23.20	22.32		
41	I	7326	13 08 39.78	29 18 50.2	21.03	20.55	1.315	Q
42	I	7567	13 08 32.10	29 19 12.0	20.51	20.34	1.812	Q
44	M	7585	13 08 42.20	29 19 14.4	25.40	22.18		
45	M	7727	13 08 28.63	29 19 26.2	22.78	22.36		
46	M	7598	13 08 02.56	29 19 14.9	23.68	22.34		
47	I	7624	13 08 16.09	29 19 17.6	19.44	19.06	1.738	Q
48	I	7822	13 07 42.64	29 19 36.5	22.21	22.01	2.458	Q
49	I	7996	13 08 32.14	29 19 52.1	22.61	21.83		
51	I	8169	13 08 01.68	29 20 09.1	21.96	21.47	0.737	Q
52	I	8184	13 08 22.09	29 20 10.5	23.86	22.63		
53	I	8222	13 07 41.37	29 20 14.9	23.81	22.48		
54	M	8212	13 07 45.40	29 20 13.8	23.46	22.95		
56	M	8659	13 08 47.08	29 20 50.3	22.16	21.55		
57	M	8754	13 09 01.20	29 20 57.4	27.34	23.15		
60	I	8845	13 07 58.75	29 21 06.2	21.99	20.85		
61	I	8890	13 08 55.51	29 21 10.5	20.96	19.05		
62	M	8965	13 08 39.81	29 21 17.8	22.92	22.72		
66	A	9215	13 08 56.26	29 21 40.6	21.71	20.41		
		9342	13 08 56.78	29 21 50.5	20.89	19.14		
67	M	9158	13 07 46.95	29 21 34.3	23.02	22.56		
68	A	9382	13 08 57.63	29 21 54.1	23.27	21.67		
		9418	13 08 57.72	29 21 57.4	22.22	20.44		
69	I	9494	13 09 16.19	29 22 03.7	16.26	15.60	0.021	G
71	M	9820	13 08 56.74	29 22 29.0	21.87	20.10		
73	I	9877	13 08 23.34	29 22 34.2	22.06	21.50	2.12	Q
76	I	9934	13 08 06.16	29 22 39.0	22.27	21.82	2.53	Q
77	I	9980	13 08 13.24	29 22 44.0	20.24	20.05	1.545	Q
79	I	G5984[d]	13 08 37.00	29 22 48.0	21.07			G
80	I	10063	13 09 07.96	29 22 52.4	23.29	22.95		
81	I	10144	13 09 00.18	29 22 58.9	20.18	18.47		
82	I	10195	13 07 33.46	29 23 03.8	20.97	19.72	0.243	BTK[e]
83	I	10304	13 08 51.82	29 23 14.7	26.21	23.39		
86	I	G55866[d]	13 08 19.05	29 23 34.8	23.93			G
88	I	10756	13 08 16.25	29 23 56.4	20.57	19.74	0.218	G
89	A	10867	13 07 57.48	29 24 06.4	23.24	23.04		
		10951	13 07 57.25	29 24 14.1	23.10	22.24		
90	A	10973	13 08 50.07	29 24 16.2	22.86	21.70		
		10953	13 08 50.34	29 24 15.0	20.96	20.07		

Table 3. continued.

SA57X	IdRank[a]	NSER[b]	RA(2000)	Dec(2000)	B_J	F	z	Class[c]
91	I	11014	13 08 27.80	29 24 20.7	17.96	16.57	0.125	G
92	I	11168	13 08 12.62	29 24 34.3	23.65	21.98		
94	I	11320	13 08 47.60	29 24 50.8	24.11	23.50		
95	I	11450	13 08 30.42	29 25 01.7	22.31	22.07	0.959	Q
96	I	11610	13 08 11.92	29 25 12.5	19.56	19.01	3.016	Q
97	I	11710	13 08 25.43	29 25 20.9	23.80	24.67		
99	I	12053	13 07 49.24	29 25 48.1	19.64	18.28	0.241	G
100	I	G48612[d]	13 07 41.85	29 26 22.9	22.19	21.85		G
101	I	G48617[d]	13 08 09.04	29 26 25.9	22.42	22.31		G
102	I	12472	13 07 29.20	29 26 25.4	22.58	20.93		
103	I	12467	13 08 34.36	29 26 28.2	20.19	19.69	0.201	G
104	M	12734	13 08 15.54	29 26 50.3	23.79	23.36		
105	I	12758	13 08 10.16	29 26 52.2	21.99	20.83		
106	I	12787	13 08 36.58	29 26 56.0	24.20	22.66		
107	A	13035	13 09 23.96	29 27 15.9	22.94	20.95		
		13088	13 09 23.71	29 27 20.2	23.40	21.47		
108	I	13155	13 08 08.73	29 27 26.8	21.71	21.06		[Q][e]
109	M	13310	13 07 56.71	29 27 38.0	21.66	21.07		
110	I	13360	13 08 13.16	29 27 43.5	22.86	22.81		
111	I	13412	13 09 06.34	29 27 48.1	22.11	21.85	2.082	Q
113	M	G55532[d]	13 08 53.56	29 27 51.1	23.81			G
114	I	13459	13 07 51.79	29 27 51.6	22.83	22.00		BTK[e]
115	I	13732	13 08 24.04	29 28 19.2	22.76	22.64		
116	I	13966	13 08 44.15	29 28 40.3	21.30	20.96	0.951	Q
117	I	13993	13 08 44.83	29 28 43.6	23.16	21.71		
118	A	14002	13 08 55.19	29 28 45.0	24.23	22.03		
		14128	13 08 55.44	29 28 57.1	21.96	20.19		
120	I	14264	13 08 03.40	29 29 08.8	20.39	18.78	0.288	BTK[e]
122	I	14630	13 08 51.24	29 29 45.4	23.82	22.93		
123	A	14733	13 08 20.29	29 29 56.3	23.21	21.93		
		14728	13 08 20.37	29 29 56.6	23.19	21.64		
		14795	13 08 20.55	29 30 01.1	20.77	19.01	0.318	G
		G59730[d]	13 08 20.02	29 29 58.1	22.98			G
		G59724[d]	13 08 20.33	29 30 02.9	20.19			G
124	A	15102	13 08 12.16	29 30 27.5	23.67	23.24		
		15093	13 08 11.92	29 30 27.7	23.38	23.29		
125	I	15180	13 08 24.40	29 30 36.9	21.13	20.71	1.797	Q
126	I	15248	13 08 42.15	29 30 43.9	22.28	21.79	1.145	Q[e]
127	I	15465	13 09 17.09	29 31 04.3	21.89	21.15		[Q][e]
131	I	16251	13 08 31.73	29 32 20.9	23.68	22.21		
134	I	16677	13 08 49.85	29 33 03.3	23.45	23.25		
135	M	16713	13 07 49.36	29 33 03.3	19.73	19.20	0.993	Q
136	I	17001	13 08 06.24	29 33 32.4	23.17	23.19		BTK[e]
137	A	17231	13 08 47.04	29 33 56.1	24.33			
		17174	13 08 47.39	29 33 50.5	23.64	22.14		
139	I	17494	13 08 33.43	29 34 23.2	23.37	22.51	0.75	RG
140	I	17750	13 08 08.51	29 34 49.1	19.79	19.23	1.179	Q

[a] Rank of optical identification: I = identified, M = marginal identification, A = ambiguous identification. [b] Serial number in the optical catalogue of the KPNO survey of SA 57 (Kron 1980; Koo 1986). [c] Q: quasar; G: galaxy; BTK extended variable object from Bershady et al. (1998); RG: radio galaxy; [Q]: point-like quasar candidate. [d] Serial number in the North Galactic Pole Faint Galaxy Catalogue (Infante et al. 1995). [e] Candidates or confirmed AGNs selected through variability and not preaviously selected by other methods.

Koo et al. (1986) list, i.e., colour selected, point-like AGN candidates. For all of them we computed the 3-σ upper limits to X-ray fluxes. The meaning of columns in Table 4 is the following: *Col. 1*: serial number NSER in the optical catalogue of KPNO survey of SA57 (Kron 1980; Koo 1986); *Cols. 2, 3*: α, δ (2000); *Col. 4*: F; *Col. 5*: redshift; *Col. 6*: 3-σ upper limit in the 2–10 keV band.

We have also considered 21 X-ray undetected objects, which were selected as AGN candidates on the basis of their optical variability: 1 point-like from Trevese et al. (1989) and 20 with diffuse images from BTK. For these objects we have computed the upper limits on the X-ray flux. Consistency of their X-ray and optical properties with the AGN character is discussed in the next section.

In summary, 21/30 = 70% of the variable candidates are not detected in X-rays; however, since 19/44 = 43% of known AGNs in our area are not detected in X-rays, we expect that a significant fraction of the variability selected candidates are genuine AGNs, but with low X/O.

Table 4. X-ray undetected optical sources.

NSER	RA(2000)	Dec(2000)	F	z	$f_x(2-10$ keV) [10^{-14} erg/cm^2/s]
5326	13 07 32.5	29 15 45	20.066	2.86	<4.16
5482	13 09 08.8	29 15 58	20.747	0.45	<1.10
5748	13 09 23.6	29 16 20	19.890	0.21	<2.04
7042	13 07 26.2	29 18 25	21.590	0.53	<3.03
7701	13 07 35.1	29 19 24	22.073	0.99	<0.75
8119	13 08 44.2	29 20 05	18.103	0.745	<0.99
8303	13 09 12.8	29 20 20	18.112	0.72	<0.91
8945	13 08 37.8	29 21 15	21.733	0.61	<0.43
9542	13 07 42.4	29 22 06	19.299	0.233	<0.87
10601	13 08 47.8	29 23 41	21.050	0.44	<0.57
11255	13 07 28.4	29 24 41	21.971	0.18	<2.91
11334	13 07 52.1	29 24 50	21.806	1.82	<0.48
11335	13 07 22.0	29 24 48	18.295	3.36	<3.44
12536	13 09 06.8	29 26 32	21.403	0.42	<1.52
12573	13 07 48.9	29 26 34	17.583	2.20	<1.31
14054	13 07 59.3	29 28 49	18.373	0.1357	<1.05
15041	13 08 03.6	29 30 20	18.331	0.137	<1.12
15437	13 09 12.7	29 31 01	18.078	2.82	<2.59
16626	13 08 13.4	29 32 55	17.820	2.95	<0.58

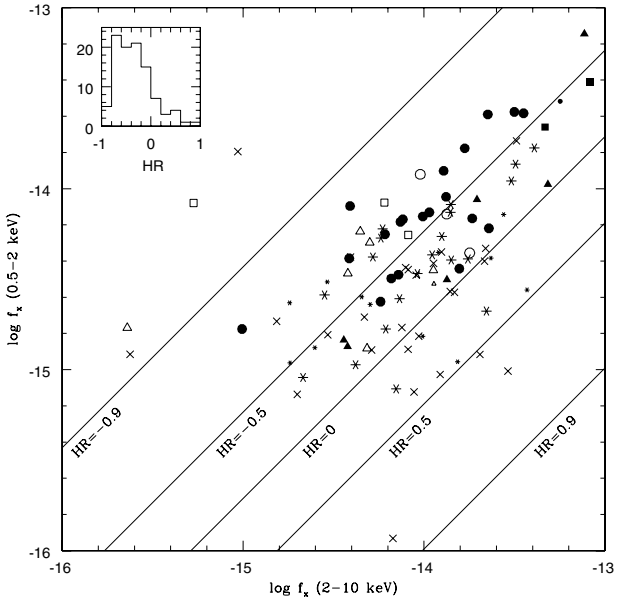

Fig. 2. $f_x(2-10)$ keV (hard band H) versus $f_x(0.5-2)$ keV (soft band S). Solid symbols: objects of known redshift; open symbols: objects without measured redshift; crosses: optically unidentified sources; asterisks: optically identified but unclassified sources; triangles: galaxies; circles: point-like AGNs; squares: variability selected AGN candidates with extended images (BTK); smaller symbols: sources with marginal (M) or ambiguous (A) identifications (see Table 2). Continuous lines represent loci of constant hardness ratio HR. The inset shows the distribution of hardness ratios.

4. Results and discussion

Figure 2 shows f_S versus f_H. Hardness ratios HR have been computed from the count rates c_S and c_H in the soft and hard band: $HR = (c_H - c_S)/(c_H + c_S)$. All confirmed QSOs/AGNs have HR in the range -0.1, -0.8. About 10% of the objects show positive HR values, suggesting absorption in the S band, as expected for type-2 objects. Most of these hard spectrum objects are optically unidentified.

Figure 3 shows the flux in the optical F band versus the 2–10 keV flux. The straight lines represent constant values of the

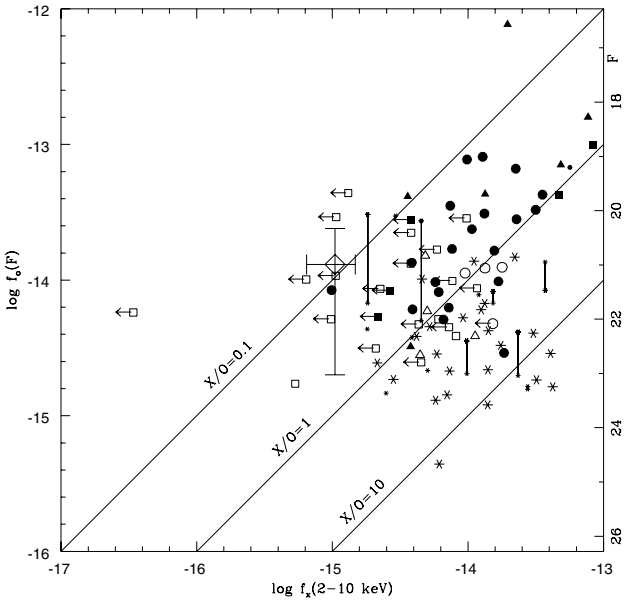

Fig. 3. Optical F band flux f_F (also shown as apparent magnitudes F) versus X-ray (2–10 keV) flux f_X(2–10 keV). Solid symbols: objects of known redshift; open symbols: objects without measured redshift; crosses: optically unidentified sources; asterisks: optically identified but unclassified sources; triangles: galaxies; circles: point-like AGNs; squares: variability selected AGN candidates with extended images (BTK); smaller symbols: sources with marginal (M) or ambiguous (A) identifications (see Table 2). Arrows: 1-σ upper limits. Connected symbols represent ambiguous identifications. Diamond with error bars represents the average fluxes of the X-ray undetected BTK objects, obtained by X-ray image stacking.

X-ray (2–10 keV) to optical (F band) flux ratio (X/O). The range of X/O ratio is wide. Considering only the confirmed AGNs with measured X-ray fluxes, the average log (X/O) is -0.24 with a standard deviation of 0.4, and corresponds to X/O = 0.58. The average X/O found by the HELLAS2XMM survey is 1.2 with a standard deviation of 0.3 (Fiore et al. 2003). The difference is mainly due to the different selection technique, since all the confirmed AGN in SA 57 were selected in the optical band. In fact the average X/O of a sample of 35 optically selected PG QSOs was found to be 0.3 with a standard deviation of 0.3 on the basis of ASCA and BeppoSAX data (Fiore et al. 2003; George et al. 2000; Mineo et al. 2000), consistent with our findings within the statistical uncertainty.

In Fig. 3, 9 objects selected on the sole basis of variability and with measured X-ray flux appear, indicated in the notes to Table 3. They show an X/O consistent with the rest of the QSO sample. Three of them (empty circles) are unconfirmed point-like objects. We assume the X-ray emission, together with the X/O typical of other AGNs/QSOs, is a confirmation of their AGN nature. A fourth variability-selected point-like object (NSER 15248) has also a spectroscopic confirmation. The other 5 variability-selected objects with a measured X-ray flux are BTK objects. The optically brightest two possess optical spectra (filled squares) and are the brightest in X-rays too. For the fainter three (open squares) again we assume that X-ray identification and X/O value confirm their AGN nature.

Optically undetected X-ray sources, indicated as crosses in Fig. 2, are not reported in Fig. 3, where they would appear as upper limits, $f_o(F) \sim 2 \times 10^{-15}$ erg cm^{-2} s^{-1}, and are discussed below.

For another 21 X-ray undetected objects selected by optical variability, one point-like and 20 with extended images (BTK), upper limits on the 2–10 keV flux are indicated by arrows. While 3-σ upper limits would be more secure, they would not be particularly significant, since most of the objects would result consistent with typical X/O of AGNs. Therefore we reported in the figure 1-σ upper limits, providing smaller X/O ratios. Still, most of these objects show $0.1 < X/O < 3$, indicating their consistency with typical AGNs. A few objects, instead, show upper limits on X/O smaller than 0.1, more consistent with X-ray emitting normal galaxies or star-burst galaxies.

As noted in Sect. 3.2, a large fraction (70%) of the objects selected by their optical variability is not detected in X-rays. A similar fraction was found by Sarajedini et al. (2006) in their *Chandra/XMM-Newton* and spectroscopic study of the Groth Westphal Survey Strip. To further investigate possible X-ray emission from our 21 undetected objects, we extracted X-ray images, in S and H bands, centred on their optical position. We then produced the corresponding stacked images, thus increasing by a factor $\sim\sqrt{20}$ the S/N ratio. In both bands a very faint "object" is visible in the centre of the stacked image. To verify that the result is not dominated by one or a few of the individual images, we have carefully inspected each of them. Only in one case (NSER 10693) there is a hint of possible photon excess respect to the local background, contributing 30% of the flux in the S band and only 1% in the H band. After the exclusion of this object the resulting fluxes in the S and H bands are $1.9 \pm 0.6 \times 10^{-16}$ and $1.0 \pm 0.4 \times 10^{-15}$ erg cm^2 s^{-1}, respectively, with a probability 1.5×10^{-4} and 4×10^{-4}, respectively, of being due to Poisson fluctuations. The average optical flux in the optical (F) band is $1.3 \pm 1.1 \times 10^{-14}$ erg cm^2 s^{-1}. The uncertainties in the X-ray fluxes are computed from the "object" and background photon counts in the stacked images; the uncertainty in the average optical flux is the standard deviation of the 20 measured fluxes. The corresponding point, representing the average X-ray undetected BTK object, lies about a factor $\gtrsim$2 below the limit of the present X-ray survey in both the S and H band and has $X/O \sim 8 \times 10^{-2}$. Its hardness ratio is about 0, i.e., relatively high but consistent with the distribution of AGN hardness ratios. Thus this average object could consist of a possibly partially absorbed AGN, hosted by a galaxy which contributes to the optical flux.

Let us consider the sample which includes all objects in the field with known redshift which are either i) X-ray detected, i.e., 35 objects with redshift in Table 3; or ii) confirmed AGNs, which were not detected in X-rays, i.e., the 19 objects of Table 4, plus 3 spectroscopically confirmed BTK objects not detected in X-rays. For all of them we can compute the optical luminosity and either the X-ray luminosity or a 3-σ upper limit, in the 2–10 keV band.

This sample contains 57 objects. Of them, 44 are QSOs, 25 of which are detected in the X-ray band. Concerning the 5 extended variable sources (BTK), two are detected in X-rays, a third, (NSER 4326) falls on a gap of the EPIC camera, another object (NSER 8553) shows both emission and absorption features and has an uncertain AGN characterisation and, lastly, for NSER 16338 the AGN character has been confirmed and the redshift measured in a new spectroscopic survey of SA 57 which is being conducted at Telescopio Nazionale Galileo (TNG) and William Herschel Telescope at La Palma (Trevese et al. 2007). The sample contains also one radio galaxy and 7 objects classified as galaxies in Munn et al. (1997).

All the above objects are reported in Fig. 4, which shows the F band luminosity $L_o(F)$ versus the 2–10 keV luminosity L_x(2–10 keV). In terms of absolute X-ray and optical luminosities, X-ray detected BTK objects populate the faint ($L_x(2-10\ \mathrm{keV}) < 3 \times 10^{43}$ erg s^{-1}) side of the diagram as expected. Objects not detected in the H band are shown in Fig. 4 as 3-σ upper limits, i.e., as robust but high X/O upper limits. Some of these objects are detected in at least one of the other X-ray bands, thus they appear in Table 2. The other upper limits, marked with big circles, correspond to the 22 above mentioned X-ray undetected objects from NED and BTK. The X-ray undetected BTK objects lie close to $L_x(2-10\ \mathrm{keV}) = 10^{42}$ erg s^{-1}, above which the X-ray emission is usually attributed to an active nucleus rather than star-burst activity. At least some of them likely have $X/O < 0.1$. Thus, selecting "variable galaxies", i.e., variable objects with diffuse images, we are indeed selecting intrinsically faint AGN, whose host galaxy is not swamped by the nuclear luminosity. The low X/O ratio may be due to the contribution of the host galaxy to the optical luminosity.

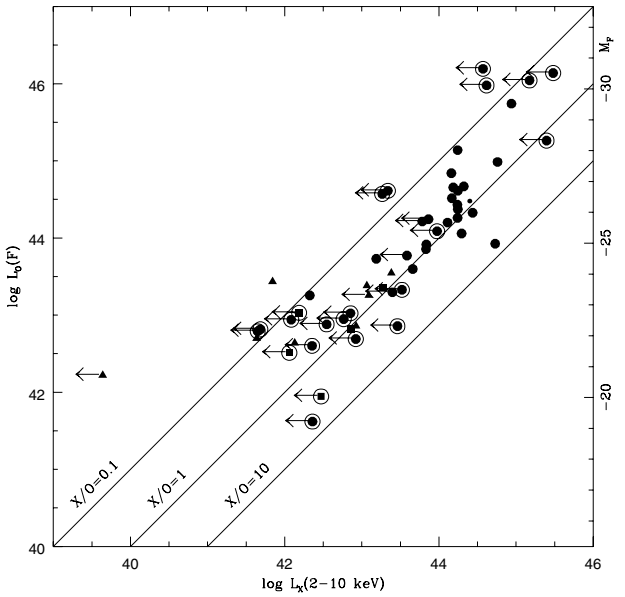

Fig. 4. Optical F band luminosity L_o versus the X-ray (2–10 keV) band luminosity L_x(2−10 keV). Luminosities are also shown as absolute magnitudes M_F; note that for the objects in figure $\langle B_J - F \rangle \simeq 0.7$. Solid symbols: objects of know redshift; triangles: galaxies; circles: point-like AGNs; squares: variability selected AGN candidates with extended images (BTK); smaller symbols: sources with marginal (M) or ambiguous (A) identifications (see Table 2). Arrows represent 3-σ (instead of 1-σ) upper limits: these occur for both X-ray undetected objects from NED and from BTK (which are marked in this figure with big circles) and for objects detected in X-ray bands other than H (without big circles). The continuous lines represent the indicated constant values of the X/O ratio.

Of the 7 X-ray detected galaxies with redshift known from Munn et al. (1997), one (SA57X 69) is a relatively nearby ($z = 0.0213$) spiral galaxy with $L_x(2-10\ \mathrm{keV}) \lesssim 4 \times 10^{39}$ erg s^{-1}. Another object is the cD galaxy at the centre of the galaxy cluster II Zw 1305.4+2941. Of the remaining 5 objects, 3 have L_x(2−10 keV) and X/O consistent with those of (faint) AGNs, while the other two have $X/O < 0.1$ and $L_x(2-10\ \mathrm{keV}) \lesssim 10^{42}$ erg s^{-1}, consistent with the luminous tail of the "normal" galaxy X-ray luminosity function (Georgantopulos et al. 2005).

Concerning the X-ray undetected point-like objects, shown in Fig. 4 as 3-σ upper limits: six (i.e., 15%) exhibit $X/O < 0.1$. This can be compared with 1% found in X-ray selected samples (see Laor et al. 1997; Fiore et al. 2003). We stress that at least two of them have $L_o(F) \gtrsim 10^{46}$ erg s^{-1}, so that the low X/O

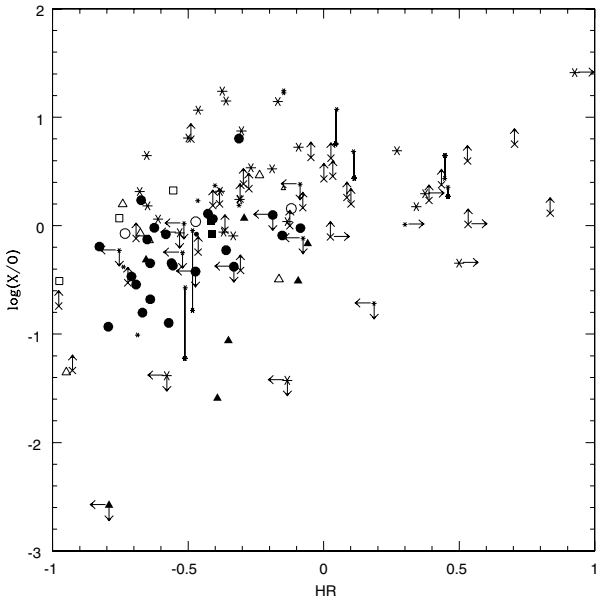

Fig. 5. X/O versus hardness ratio *HR*. Solid symbols: objects of know redshift; open symbols: objects without measured redshift; crosses: optically unidentified sources; asterisks: optically identified but unclassified sources; triangles: galaxies; circles: point-like AGNs; squares: variability selected AGN candidates with extended images (BTK); smaller symbols: sources with marginal (M) or ambiguous (A) identifications (see Table 2), connected in the case of ambiguous identifications. Horizontal and downward vertical arrows: 3-σ upper limits derived from X-ray bands; upward vertical arrows: optical limit $F > 22$.

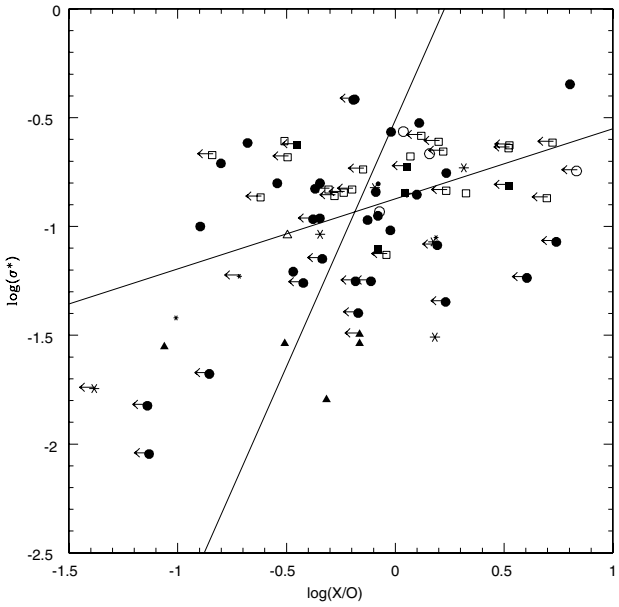

Fig. 6. Logarithm of the optical variability, as measured by the the rms magnitude changes σ^*, versus the logarithm of the X/O ratio. Symbols as in the previous figures. Arrows: 3-σ upper limits.The regression lines shown are computed excluding the upper limits.

cannot be due to the contribution of the host galaxy to the optical light, as in the case of fuzzy objects, but must be intrinsic to the nuclear component.

In Fig. 5 we report the X/O ratio versus the hardness ratio *HR* for all of the objects detected in at least two of the S, H, T bands. Horizontal and downward vertical arrows are also reported to indicate X-ray limits when the relevant detections are missing. The X-ray detected objects not seen in the optical F band have X/O ratios reported as lower limits assuming $F = 22$ as the limiting magnitude (where the optical sample is ∼50% complete). Some of these objects have higher X/O in comparison to the rest of the sample, consistent with being obscured in the optical and soft X-ray bands, but not in hard X-rays.

While optically undetected objects (crosses) are spread over the entire *HR* range, their fraction is higher among the hard (e.g. $HR > 0$) objects. This is consistent with the analysis of Szokoly et al. (2004), which is deeper than ours both in X-ray and optical bands, and shows that hard X-ray objects have on average fainter optical magnitudes.

Thus, objects lying in the upper right of the figure, e.g., X/O $\gtrsim 3$ and $HR \gtrsim 0$, are good type-2 AGN candidates, where the nuclear component is obscured and the colour is dominated by the light from the host galaxy. Such objects are not selected as AGN candidates from optical observations (i.e., on the basis of non-stellar colours or variability), while they are detected in the X-ray band. The other optically identified objects (asterisks) require optical spectroscopy to discriminate among starburst galaxies, AGNs or normal X-ray emitting galaxies.

In Fig. 6 we report the variability amplitude σ^* measured by the rms magnitude changes (Trevese et al. 1989; Bershady et al. 1998) versus the X/O ratio. Point-like objects were classified as variable for $\sigma* > 0.1$ mag, while the variability threshold for extended objects was in the range 0.06–0.2 mag, depending on the object magnitude (Trevese et al. 1989; Bershady et al. 1998). Data in Fig. 6 are reported both for variable and non variable objects.

For the objects with measured X/O a Pearson correlation coefficient $r = 0.38$ is found, with a probability of the null hypothesis $P(>r) = 0.02$.

Since the fraction of objects with only upper limits on X/O is about 50%, we also computed both the Kendall τ and the Spearman ρ rank correlation coefficients as generalised for application to censored data (see e.g. Isobe et al. 1986; Akritas & Siebert 1996)) adopting 3-σ upper limits on X/O. The results is: $\tau = 0.26$ with $P(>\tau) = 0.011$ and $\rho = 0.31$ with $P(>\rho) = 0.007$. To check to what extent the above results rely on the most deviant point on the top right of Fig. 6 (SA57X 33, a quasar at $z = 2.124$), we re-evaluated the rank correlations after removing this object from the list. The results ($\tau' = 0.22$ with $P(>\tau') = 0.03$ and $\rho' = 0.27$ $P(>\rho') = 0.017$) do not change substantially and remain moderately significant (a 2.4-σ result if the probability distribution were Gaussian). We note that, on average, optical AGN variability decreases with luminosity as $\sigma^* \propto L^{-0.25}$ (Vanden Berk et al. 2004), while the X-ray to optical ratio decreases with luminosity as X/O $\propto L^{-\chi}$ with $\chi \approx 0.25-0.45$ (Strateva et al. 2005; Vignali et al. 2006; Miyaji et al. 2006). It is still unclear whether the X/O-luminosity anticorrelation reflects some physical property of the AGNs or is simply due to a selection effect. In both cases this correlation is qualitatively consistent with our results showing an increase of variability with the X-ray to optical ratio. This suggests to further investigate the X/O-σ^* correlation and its possible physical origin.

5. Summary

– We have surveyed with XMM-Newton a ∼0.2 deg^2 area in the field of SA 57 down to flux limits of 10^{-15}, 5×10^{-16}, 2×10^{-15}, 10^{-14} erg cm^{-2} s^{-1} in the (0.5–10 keV) (T),

(0.5–2 keV) (S), (2–10 keV) (H), and (5–10 keV) (HH) band respectively.
- Adopting a threshold probability of 2×10^{-5} of detecting Poisson fluctuations of the Background, we found 119, 117, 58, 6 sources in the T, S, H, and HH bands respectively.
- The distribution of X-ray to optical flux ratios shows an excess of low X/O among optically selected AGNs in agreement with previous studies of optically selected PG QSOs (Fiore et al. 2003).
- We detect X-ray emission from 9 objects selected on the sole basis of variability. We assume this is a confirmation of their AGN character. Three of them (1 point-like and 2 extended) also possess optical spectra consistent with their AGN nature.
- Variability selected, but X-ray undetected objects show 1-σ upper limits on X/O consistent with the AGN population. The stacked image of these objects indicates average X-ray fluxes of $1.9 \pm 0.6 \times 10^{-15}$ and $1.0 \pm 0.4 \times 10^{-17}$ erg cm^2 s^{-1} in the S and H bands respectively, significant at more than 3-σ level, corresponding to a low X/O $\sim 8 \times 10^{-2}$ and $HR \sim 0$.
- Of the known QSOs in the field only 25/44 are detected in X-rays.
- On the basis of 3-σ upper limits, 15% of QSOs have X/O $<$ 0.1, compared to only 1% of X-ray selected samples.
- Low X/O in objects with $L_o(F) \gtrsim 10^{46}$ erg s^{-1} must be intrinsic of the nuclear component rather than due the host galaxy light.
- Most X-ray selected objects, not previously identified as AGNs, are probably type-2 objects dominated by the stellar components.
- The optical variability appears marginally correlated with the X/O ratio. This could be explained by the decrease with luminosity of both X/O and variability.
- From this survey we will derive in a forthcoming paper an estimate of the space density of LLAGNs after further progress of the ongoing spectroscopic survey of SA57 (Trevese et al. 2007).

Acknowledgements. We thank Valentina Zitelli for useful discussions. We thank the referee, Vicki Sarajedini, for remarks and suggestions. We acknowledge partial support of Agenzia Spaziale Italiana and Istituto Nazionale di Astrofisca by the grant ASI/INAF n. I/023/05/0. This research has made use of the NASA/IPAC Extragalactic Database (NED) which is operated by the Jet Propulsion Laboratory, California Institute of Technology, under contract with the National Aeronautics and Space Administration.

References

Alexander, D. M., Bauer, F. E., Brandt, W. N., et al. 2003, ApJ, 126, 539
Akritas, M. G., & Siebert, J. 1996, MNRAS, 278, 919
Anderson, S. F., Fan, Xiaohui, & Richards, G. T. 2001, AJ, 122, 503
Becker, R. H., White, R. L., & Helfand, D. J. 1995, ApJ, 450, 559
Bershady, M. A., Trevese, D., & Kron, R. G. 1998, ApJ, 496, 103 (BTK)
Brandt, W. N., & Hasinger, G. 2005, ARA&A, 43, 827
Cavaliere, A., & Vittorini, V. 2002, ApJ, 570, 114
Comastri, A., Mignoli, M., Ciliegi, P., et al. 2001, MNRAS, 327, 781
Cowie, L. L., Barger, A. J., Bautz, M. W., Brandt, W. N., & Garmire, G. P. 2003, ApJ, 584, L57
Cristiani, S., Trentini, S., La Franca, F., et al. 1996, A&A, 306, 395
Croom, S. M., Smith, R. J., Boyle, B. J., et al. 2001, MNRAS, 322, L29
Damiani, F., Maggio, A., Micela, G., & Sciortino, S. 1997a, ApJ, 483, 350
Fan, Xiaohui, Strauss, M. A., & Schneider, D. P. 2001, AJ, 121, 54
Ferrarese, L., & Merrit, D. 2000, ApJ, 539, L9
Fiore, F., Brusa, M., Cocchia, F., et al. 2003, A&A, 409, 79
Georgantopulos, I., Geogakakis, A., & Koulouridis, E. 2005, MNRAS, 360, 782
George, I. M., Turner, T. J., Yaqoob, T., et al. 2000, ApJ, 351, 52
Hasinger, G. 2003, AIPC, 666, 227
Hickox, R. C., & Markevitch, M. 2006, ApJ, 645, 95
Hook, I. M., McMahon, R. G., Boyle, B. J., & Irwin, M. J. 1994, MNRAS, 268, 305
Infante, L., Pritchet, C. J., & Hertling, G. 1995, J. Astron. Data (JAD), 1, 2
Isobe, T., Feigelson, E. D., & Nelson, P. I. 1986, ApJ, 306, 490
Koo, D. C. 1986, ApJ, 311, 651
Koo, D. C., & Kron, R. G. 1988, ApJ, 325, 92
Koo, D. C., Kron, R. G., & Cudworth, K. M. 1986, PASP, 98, 285
Kormendy, J., & Richstone, D. 1995, ARA&A, 33, 581
Kron, R. G. 1980, ApJS, 43, 305
La Franca, F., Fiore, F., Comastri, A., et al. 2005, ApJ, 635, 864
Laor, A., Fiore, F., Elvis, M., Wilkes, B. J., & McDowell, J. C. 1997, ApJ, 4777, 93
Linden-Vornle, M. J. D., Norgaard-Nielsen, H. U., Jorgensen, H. E., et al. 2000, A&A, 359, 51
Marconi, A., & Hunt, L. K. 2003, ApJ, 589, L21
Mineo, T., Fiore, F., Laor, A., et al. 2000, A&A, 359, 471
Miyaji, T., Connolly, A. J., Szalay, A. S., & Boldt, E. 1997, A&A, 323, L37
Miyaji, T., Hasinger, G., Lehmann, I., & Schneider, D. P. 2006, AJ, 131, 659
Moretti, A., Campana, S., Lazzati, D., & Tagliaferri, G. 2003, ApJ, 588, 696
Munn, J. A., Koo, D. C., Kron, R. G., et al. 1997, ApJS, 109, 45
Pillitteri, I., Micela, G., Damiani, F., & Sciortino, S. 2006, A&A, 450, 993
Puccetti, S., Fiore, F., D'Elia, V., et al. 2006, A&A, 457, 501
Sarajedini, V. L., Gilliland, R. L., & Kasm, C. 2003, ApJ, 599, 173
Sarajedini, V. L., Koo, D. C., Phillips, A. C., et al. 2006, ApJS, 166, 69
Schmidt, M., Schneider, D. P., & Gunn, J. E. 1995, AJ, 110, 68
Silk, J., & Rees, M. J. 1998, A&A, 331, L1
Steffen, A. T., Strateva, I., Brandt, W. N., et al. 2006, AJ, 131, 2826
Strateva, I. V., Brandt, W. N., Schneider, D. P., Vanden Berk, D. G., & Vignali, C. 2005, AJ, 130, 387
Struder, L., Briel, U., Dennerl, K., et al. 2001, A&A, 365, L18
Szokoly, G. P., Bergeron, J., Hasinger, G., et al. 2004, ApJS, 155, 271
Tang, S., Zhang, S. N., & Hopkins, P. F. 2007 [arXiv:astro-ph/0702082]
Tremaine, S., Gebhardt, K., Bender, R., et al. 2002, ApJ, 574, 740
Trevese, D., Pittella, G., Kron, R. G., Koo, D. C., & Bershady, M. A. 1989, AJ, 98, 108 (T89)
Trevese, D., Kron, R. G., Majewski, S. R., Bershady, M. A., & Koo, D. C. 1994, ApJ, 433, 494 (T94)
Trevese, D., Kron, R. G., & Bunone, A. 2001, ApJ, 551, 103
Trevese, D., Vagnetti, F., Zitelli, V., Boutsia, K., & Stirpe, G. 2007, in preparation
Turner, M. J. L., Abbey, A., Arnaud, M., et al. 2001,A&A, 365, L27
Vanden Berk, D. E., Wilhite, B. C., Kron, R. G., et al. 2004, ApJ, 601, 692
Vignali, C., Brandt, W. N., & Schneider, D. P. 2006, AJ, 131, 659
Vittorini, V., Shankar, F., & Cavaliere, A. 2005, MNRAS, 363, 1376
Warren, S. J., Hewett, P. C., & Osmer, P. S. 1994, ApJ, 421, 412
Wolf, C., Wisotzki, L., Borch, A., et al. 2003, A&A, 408, 499